PHOTONICS Research

Enhanced light emission from AlGaN/GaN multiple quantum wells using the localized surface plasmon effect by aluminum nanoring patterns

Kyung Rock Son,[1] Byeong Ryong Lee,[1] Min Ho Jang,[2] Hyun Chul Park,[2] Yong Hoon Cho,[2] and Tae Geun Kim[1,*]

[1]School of Electrical Engineering, Korea University, Anam-ro 145, Seongbuk-gu, Seoul 02841, South Korea
[2]Department of Physics and KI for the NanoCentury, Korea Advanced Institute of Science and Technology, Daejeon 305-701, South Korea
*Corresponding author: tgkim1@korea.ac.kr

Received 12 September 2017; revised 11 November 2017; accepted 11 November 2017; posted 15 November 2017 (Doc. ID 305263); published 14 December 2017

We investigate the localized surface plasmon (LSP) effect by Al nanorings on the AlGaN/GaN multiple quantum well (MQW) structure emitting at 365 nm. For this experiment, first, the size of Al nanorings is optimized to maximize the energy transfer (or coupling) between the LSP and MQW using the silica nanospheres. Then, the Al nanorings with an outer diameter of 385 nm, which exhibit a strong absorption peak in the near-ultraviolet region, are applied to the top surface of the AlGaN/GaN MQW. The photoluminescence (PL) intensity of the MQW structure with Al nanorings increased by 227% at 365 nm compared to that without Al nanorings. This improvement is mainly attributed to an enhanced radiative recombination rate in the MQWs through the energy-matched LSPs by the temperature-dependent PL and time-resolved PL analyses. The radiative lifetime was about two times shorter than that of the structure without Al nanorings at room temperature. In addition, the measured PL efficiency at room temperature of the structure with Al nanorings was 33%, while that of the structure without Al nanorings was 19%, implying that LSP-QW coupling together with the nanoring array pattern itself played important roles in the enhancement.

OCIS codes: (240.6680) Surface plasmons; (230.3670) Light-emitting diodes; (250.5230) Photoluminescence.

https://doi.org/10.1364/PRJ.6.000030

1. INTRODUCTION

Ultraviolet (UV) light-emitting diodes (LEDs) have been used in several applications such as chemical sensors for the detection of biohazardous and heavy metals, optical communication, and water purification systems [1–5]. However, the external quantum efficiency (EQE) of UV LEDs is still much lower than that of blue and green LEDs. This is because UV LEDs have AlGaN layers in their active layers, which are strongly influenced by the nonradiative recombination process via the high density of threading dislocations and polarization fields related to the quantum-confined stark effect (QCSE). These effects lower the internal quantum efficiency (IQE) of UV LEDs and eventually result in low EQEs [6–8]. Thus, to fundamentally improve the EQE of UV LEDs, it is important to enhance the IQE in addition to the light extraction efficiency of UV LEDs.

The study of improving the IQE of UV LEDs is closely related to the improvement of crystal quality by reducing the polarization charges existing in the epitaxial layer structure [i.e., via control of the QCSE in quantum wells (QWs) or reduction of lattice mismatch using GaN bulk substrates] [9–11]. Through these efforts, the IQE of deep-UV LEDs has improved up to 80% or more at room temperature [9]. However, the maximum EQE of UV LEDs is still low—for example, approximately 30% [4] for 365 nm near-UV LEDs and 20% [12] for 275 nm deep-UV LEDs.

Many research groups have investigated various methods that can enhance both the IQE and EQE simultaneously using localized surface plasmons (LSPs) [13–18] and/or embedded photonic crystals [19–21] using various shapes of metal nanoparticles or nanostructures. Hong *et al.* reported the enhancement of light emission and IQE of near-UV LEDs by using colloidal silver nanoparticles on a p-GaN spacer layer to induce the LSPs [15]. Huang *et al.* showed a significant increase in the photoluminescence (PL) of AlGaN-based multiple QW (MQW) LEDs using cube-shaped Al nanoparticles when the light waves are coupled to the LSPs [16]. Yin *et al.* also reported the enhancement of deep-UV emission by introducing the energy-matched coupling of LSPs from Al-based triangular prism nanostructures with hot excitons in QWs [17].

On the other hand, among the studies on nanostructure patterns for LSPs, nanoring patterns have been reported to generate high local electric fields from LSP modes intensively coupled between the inner and outer surface, due to resonant excitation of its dominant dipole-active plasmon resonance and uniformly distributed field in the cavity inside the ring. Also, these structures create two plasmonic modes (a low-energy "bonding" mode and high-energy "anti-bonding" mode), resulting in a high degree of tunability [22,23].

In this study, we investigate the effect of an Al nanoring structure on the light extraction efficiency from AlGaN/GaN MQWs of 365 nm LEDs through the LSP coupling effect. Note that the SP energy of Al ranges from 3.4 to 4 eV (310–365 nm) [24]. First, we investigate the LSP resonance absorption spectra for different size of Al nanorings. Then, we chose the appropriate Al nanoring size that could interact with the light emitted from the 365 nm LEDs and confirmed that the PL intensity was increased. In addition, temperature-dependent PL (TDPL) and time-resolved PL measurements were conducted to investigate the carrier dynamics of the recombination mechanism. These systematic analyses, including the PL efficiency and carrier lifetime, indicate that the improvement in IQE can be attributed to the LSP-QW coupling and the nanoring pattern formed at the sample surface.

2. EXPERIMENTAL DETAILS

A. Methods of Characterization

The morphology of the Al nanoring array was characterized using scanning electron microscopy (SEM, Hitachi, s-4300). The morphology and height distribution of the Al nanoring array were measured by atomic force microscopy (AFM, Park XE 15). Cross-sectional images of the AlGaN/GaN MQW structure and Al nanorings were obtained using a high-angle annular dark-field (HAADF) scanning transmission electron microscope (STEM) with energy dispersive X-ray spectroscopy (EDS) analysis at an accelerating voltage of 200 kV (FEI, Talos F200X). The absorbance spectra of the Al nanoring array were measured using a UV-visible spectrophotometer (Perkin Elmer, Lambda 35). PL measurements were performed using a pulse laser operating at a wavelength of 266 nm with an average output power of 10 mW. Time-resolved PL measurements were performed using a mode-locked femtosecond pulsed Ti:sapphire laser (Coherent, Chameleon Ultra II) and a streak camera detector (Hamamatsu, C7700-01). The excitation source at 266 nm was prepared by the third-harmonic-generation method, and the width and repetition of the laser were 150 fs and 4 MHz, respectively. We used a cryostat to control the temperature between 12 and 300 K.

B. Fabrication of 365 nm AlGaN/GaN LEDs with Al Nanorings

The light-emitting structure was grown via metal organic chemical vapor deposition on *c*-plane sapphire substrates. After the growth of a 50 nm thick AlN buffer layer and 1000 nm thick undoped $Al_{0.1}Ga_{0.9}N$ layer on the sapphire substrates, a 2000 nm thick n-type $Al_{0.1}Ga_{0.9}N$ layer was grown. An AlGaN MQW array, which consisted of four periods of 2.5 nm thick, undoped GaN wells and 10 nm thick n-type $Al_{0.1}Ga_{0.9}N$ barriers, was subsequently grown. Finally, a 10 nm thick undoped-$Al_{0.1}Ga_{0.9}N$ EBL was grown and covered with a 20 nm thick p-type $Al_{0.2}Ga_{0.8}N$ layer and 150 nm thick p-type $Al_{0.1}Ga_{0.9}N$ capping layer. The fringing electric field of LSPs has a limiting distance, which is Z (penetration depth) and can be given by

$$Z = \lambda/(2\pi)[(\varepsilon_s' - \varepsilon_m')/\varepsilon_m'^2]^{1/2}, \quad (1)$$

where ε_s' and ε_m' represent the real part of the dielectric constant of the semiconductor and metal, respectively [13]. In our case, $Z = 16$ nm was calculated at a wavelength of 365 nm for Al ($\varepsilon_m' = -19$) on the GaN layer ($\varepsilon_s' = 8.9$). Thus, we removed all p-type layers on the EBL layer using the inductively coupled plasma (ICP) reactive-ion etching (RIE) process. In order to fabricate the Al nanorings, the nanosphere lithography (NSL) method was used. The NSL method has the advantages of being inexpensive and a simple technique for producing size-tunable metal nanoparticles with controllable plasmon resonances in the deep-UV to infrared region [25,26]. Figure 1(a) shows a flow chart illustrating the Al nanoring array fabrication process on the near-UV LED AlGaN/GaN MQW structure using the NSL method.

Initially, we synthesized SiO_2 nanospheres with diameters of 300 nm using tetraethyl orthosilicate, ethanol (C_2H_5OH), ammonia (NH_3), and deionized water by the solgel method at room temperature. Then, we arranged the SiO_2 nanosphere monolayer on top of the MQWs by using the spin coating method. After spin coating, a 25 nm thick Al film was deposited on the prepared wafer with the SiO_2 nanospheres using the radio-frequency sputtering technique. Next, the wafer was exposed to Cl_2 and Ar etching gas by using the ICP-RIE process. Finally, the exposed SiO_2 nanospheres were etched under O_2 and SF_6 etching gas by using the RIE process, resulting in the Al nanoring patterns.

C. Finite-Difference Time-Domain Simulation

Three-dimensional finite-difference time-domain (3D FDTD) simulations using the FullWAVE software package (Synopsys and Rsoft Group, Inc.) were performed to obtain the absorbance spectrum and near-electromagnetic field distribution of the Al nanoring array to analyze the plasmonic modes by LSP resonance. The structure for the simulation consisted of an Al nanoring with a width of 65 nm, height of 60 nm, and outer diameter of 385 nm with a hexagonal close-packed (HCP) unit cell. A pulse-mode source with TE and TM waves was used to obtain the wavelength-resolved response for the Al nanoring structure.

3. RESULTS AND DISCUSSION

Figures 1(b)–1(d) show SEM top-view images of the Al nanoring single layers with the HCP structure, fabricated by the NSL and subsequent etching process using SiO_2 nanospheres. In this process, some of the top layers were etched unintentionally with SiO_2 nanospheres. This might be able to influence the light extraction efficiency from MQWs. The Al nanorings were prepared uniformly and closely with average diameters of 165, 385, and 520 nm. Figures 1(e)–1(g) present the absorbance spectra of the experimental results. A blueshift of the corresponding peak is observed as the size of the Al nanorings

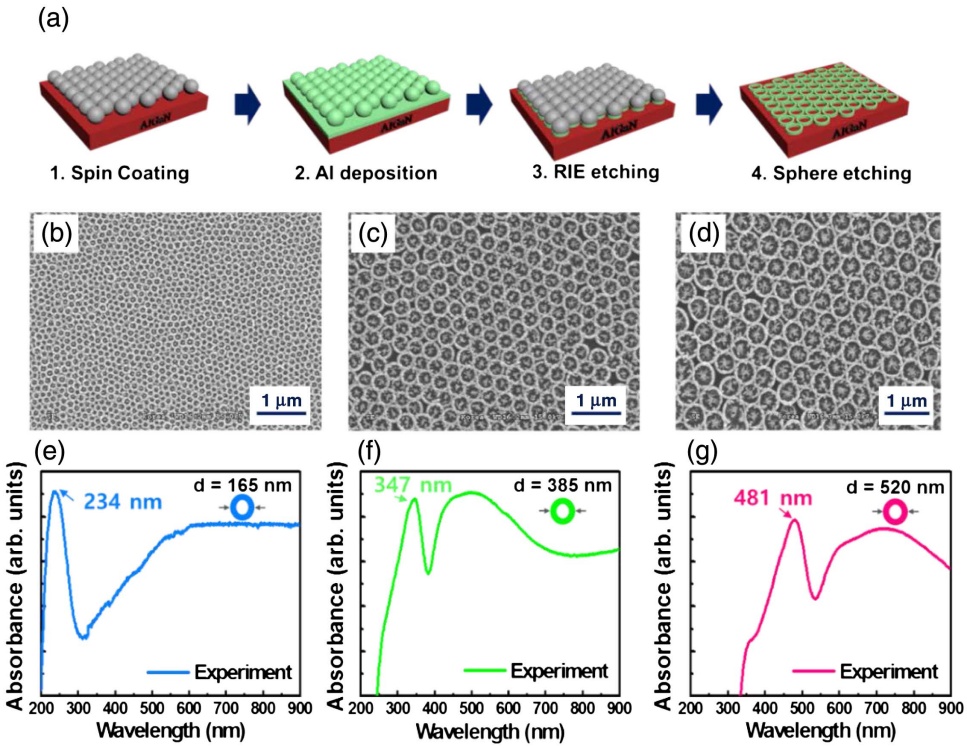

Fig. 1. (a) Schematics of the processing steps used to fabricate Al nanoring arrays using SiO_2 nanospheres. (b)–(d) SEM images showing top views of Al nanoring arrays fabricated using SiO_2 nanospheres with diameters of 150, 300, and 450 nm, respectively. (e)–(g) Experimental absorbance spectra of the Al nanorings with outer diameters of 165, 385, and 520 nm, respectively.

decreases. In addition, the plasmonic hybrid coupling of the nanoring structure between the inner and outer surfaces with two plasmon modes is represented well. Among these Al nanorings, we have better structural analysis of the 385 nm diameter Al nanoring pattern, which can interact with the light emitted at a wavelength of 365 nm from the AlGaN/GaN MQW structure.

Figure 2(a) shows a schematic of the AlGaN/GaN-based MQW structure with Al nanorings. To evaluate the height distribution of the 385 nm diameter Al nanorings, an AFM image was measured, as shown in Fig. 2(b). The height distribution ranges from −80 to +60 nm with a maximum (frequency) at about 20 nm. Therefore, we think that the real height of the 385 nm diameter Al nanorings is approximately 100 nm when the point of −80 nm is assumed to be zero. However, this AFM image-based height calculation has some errors because it includes the depth of the etched substrate. Therefore, TEM cross-section and its corresponding EDS mapping images of Al element (green color) were captured, and the actual height of the Al nanorings was confirmed as 60 nm, as shown in Figs. 2(c) and 2(d). This implies that the factor affecting the height of the nanorings is not the thickness of the metal film but the size of the SiO_2 nanosphere because the metal atoms sputtered by Ar ions randomly move and deposit at the surface of the SiO_2 nanospheres during the sputtering process. Then, during the Al etching process, Al metal on the upper side of the SiO_2 nanosphere was etched, while the Al metal deposited below the overhang of the nanosphere remained, which determines the height of the nanorings. Furthermore, we numerically modeled the 385 nm diameter Al nanoring structure in order to theoretically analyze it using the 3D FDTD method.

Figure 3(a) shows a schematic of the 385 nm diameter Al nanoring–HCP unit cell with a periodic boundary condition layer along the x- and y-axis directions and a perfectly matched layer along the z-axis directions. Figure 3(b) presents the normalized extinction spectra of the Al nanoring array–HCP structure calculated for both TE- and TM-polarized waves. The TE-polarized waves matched well with the experimental result of Fig. 1(f), and two peaks related to the LSP mode were observed for both TE and TM waves. Note that the low-energy "bonding" mode is typically located in the visible or near-infrared region, while the high-energy asymmetric "anti-bonding" mode is typically located near the UV region, as the result of the plasmon hybridization by nanoring structures [22,27]. In order to apply the Al nanoring array to the AlGaN/GaN MQW structure emitting at 365 nm, we chose the high-energy plasmonic mode ("anti-bonding" mode).

A high-energy plasmonic mode naturally has an electric field distribution in the metal because of the asymmetrical distribution of charges located on the outer and inner surfaces of the rings [23]. However, in our case, a strong electric field distribution was observed on the outer surfaces, whereas a weak electric field was distributed in the metal, as shown in Figs. 3(c) and 3(d). This strong electric field is attributed to the interaction of adjacent rings because the spaces between the rings are shorter than the width of the rings. In addition, the TE-polarized waves interacted more effectively with Al

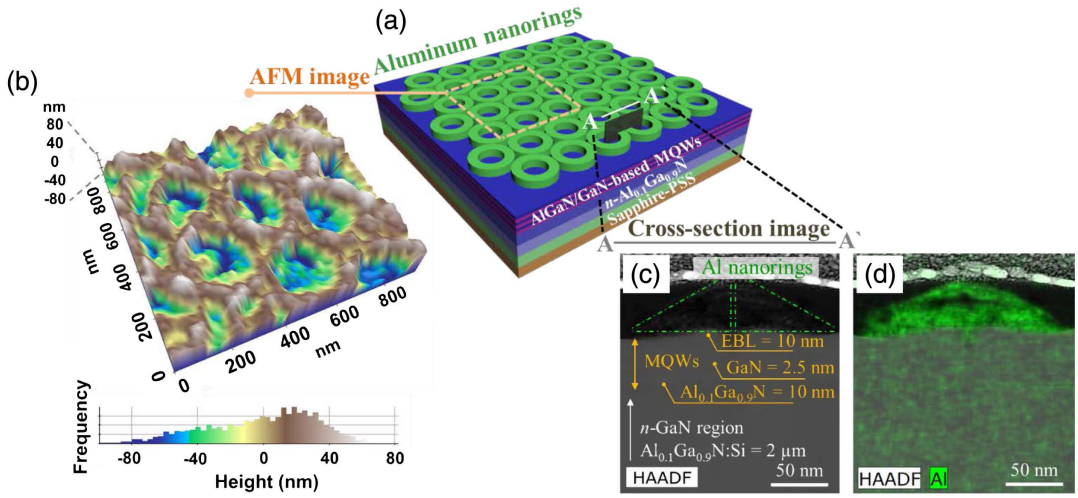

Fig. 2. (a) Schematic of the AlGaN/GaN-based near-UV LED structure with Al nanorings to capture both AFM and TEM images. (b) AFM image of the top surface of the near-UV LED with 385 nm Al nanorings that have an HCP array structure and height distribution. (c) STEM cross-sectional image of the AlGaN/GaN-based near-UV LED with Al nanorings and (d) the corresponding EDS mapping image of Al element (green color).

nanorings compared with the TM-polarized waves because the extinction peak (high-energy plasmonic mode) of the TE mode was matched well with the emission wavelength of the sample, and its maximum magnitude of the electric field distribution was higher than that of the TM mode. To estimate the penetration depth of the LSP mode, we calculated the electric field distribution around Al nanoring arrays at the position of the z axis at $z = 0$ nm (the point where the electric field of the LSP mode starts) and $z = -16$ nm [penetration depth estimated by the Eq. (1)], as shown in Figs. 3(a), 3(c), and 3(e). As a result, interestingly, the penetration depth of the LSP mode by the simulated electric field mapping was found to be almost the same as the value (= 16 nm) calculated by the Eq. (1) because the maximum magnitude of the electric field at $z = -16$ nm [1.81, see Fig. 3(e)] corresponds to the 1/e decay value of the maximum magnitude of the electric field at $z = 0$ nm [4.92, see Fig. 3(c)]. From the distribution of magnetic fields in Fig. 3(f), we can also confirm that the plasmonic modes are formed on the outer surfaces of the rings via the intensity profile of the magnetic fields.

Based on these simulated results, we have applied the Al nanoring array—HCP structure to the near-UV LED

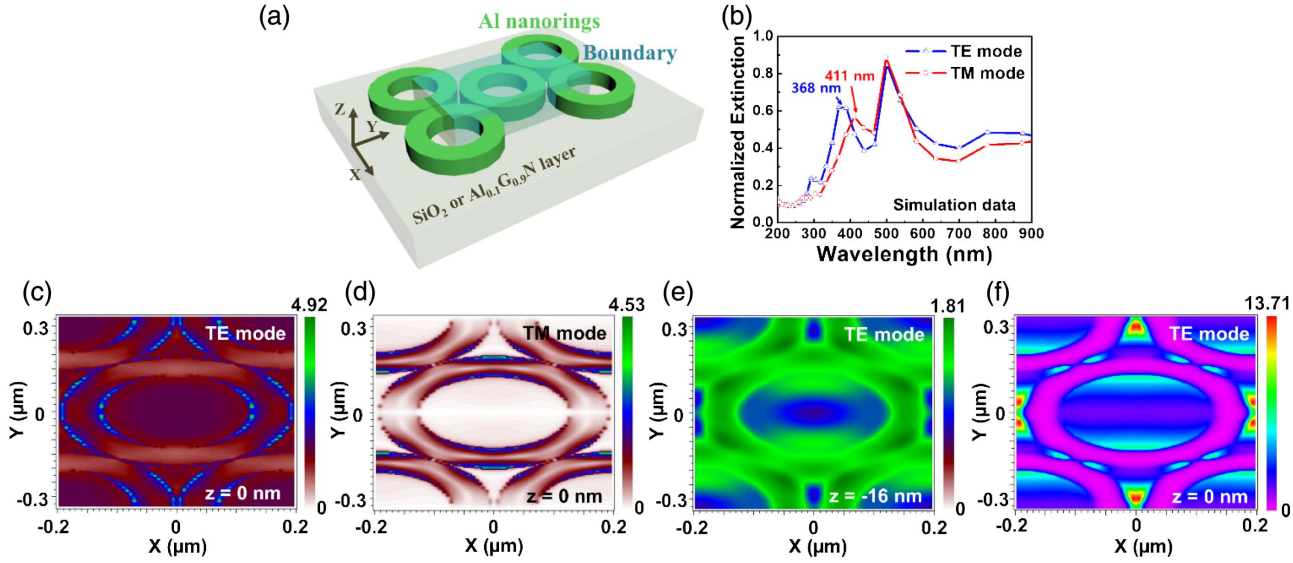

Fig. 3. 3D FDTD simulations of the Al nanoring array, which has an HCP structure with outer diameters of 385 nm, plasmonic system. (a) Schematic of the simulated Al nanoring array–HCP unit cell structure. (b) Simulated absorbance spectra of the Al nanoring array with an HCP unit cell on the glass substrate, when the incident light was both TE and TM polarized. Top views of the local electric field distributions of Al nanorings with HCP unit cell on the $Al_{0.1}Ga_{0.9}N$ substrate, when using dipole modes of (c) TE and (d) TM at $z = 0$ nm, and (e) TE at $z = -16$ nm, respectively, at 365 nm. (f) Intensity profile of the magnetic field at 365 nm.

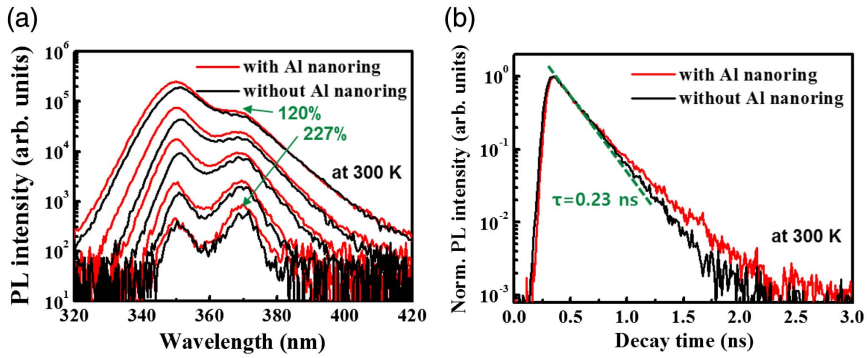

Fig. 4. (a) Power-dependent PL measurements with source power of 0.03, 0.1, 0.5, 2, and 8 mW from bottom to top. (b) Time-resolved PL spectra of the AlGaN/GaN MQW structure with and without Al nanorings at room temperature.

sample in order to confirm the characteristic of PL and optical properties.

Figure 4(a) shows the power-dependent PL intensity of the near-UV LED AlGaN/GaN MQW structures with and without Al nanorings at room temperature by changing the source power from 0.03 to 8 mW transmitted by a 266 nm laser. A 227% enhancement in peak PL intensity is observed using a source power of 0.03 mW at a wavelength of 365 nm. When the source power is 8 mW, a 120% enhancement is obtained from the sample with the Al nanoring structure compared with the sample without the Al nanoring structure. The PL spectrum of our samples exhibits peaks at 350 nm, which represents the emission of the p-AlGaN capping layer. Figure 4(b) presents the time-resolved PL spectra of the AlGaN/GaN MQWs with and without Al nanorings at room temperature. The PL lifetime can be expressed as

$$1/\tau_m = 1/\tau_r + 1/\tau_{nr}, \tag{2}$$

where τ_m, τ_r, and τ_{nr} are the measured lifetime, radiative lifetime, and nonradiative lifetime, respectively. The lifetimes measured for both samples were almost identical to be 230 ps at the 1/e position of the normalized PL intensity. In general, the τ_m would be shorter by adding the Al nanorings because of the LSP-QW coupling; however, it was almost the same for our case. Therefore, carrier dynamics related to radiative and nonradiative recombination lifetime were investigated to understand why the τ_m was almost identical for both samples while the PL intensity was enhanced at room temperature for the sample with Al nanorings.

To investigate the carrier dynamics of recombination in the samples with and without Al nanorings, TDPL measurements with time-resolved PL were performed in the temperature range from 17 to 300 K, as shown in Fig. 5(a). In addition, we deduced the radiative and nonradiative lifetime from the integrated PL intensity and τ_m measured as a function of temperature, systematically. Figures 5(b) and 5(c) describe the temperature dependences of τ_m, τ_r, and τ_{nr} for the samples without [see Fig. 5(b)] and with Al nanorings [see Fig. 5(c)]. The relationship of

$$\eta_{\text{int}}(T) = \tau_m(T)/\tau_r(T) = 1/[1 + \tau_r(T)/\tau_{nr}(T)], \tag{3}$$

was used assuming an IQE of 100% at 10 K [28,29]. Surprisingly, over the measured temperature range, a noticeable reduction in extracted radiative lifetimes (τ_r) is found for the sample with Al nanorings compared with that without Al nanorings. At room temperature, τ_r is 0.63 ns for the sample with Al nanorings and 1.24 ns for that without Al nanorings. In contrast, the τ_{nr} of the sample without Al nanorings was calculated as 0.28 ns, while that of the sample with Al nanorings was 0.36 ns. This result can be explained by the passivation of

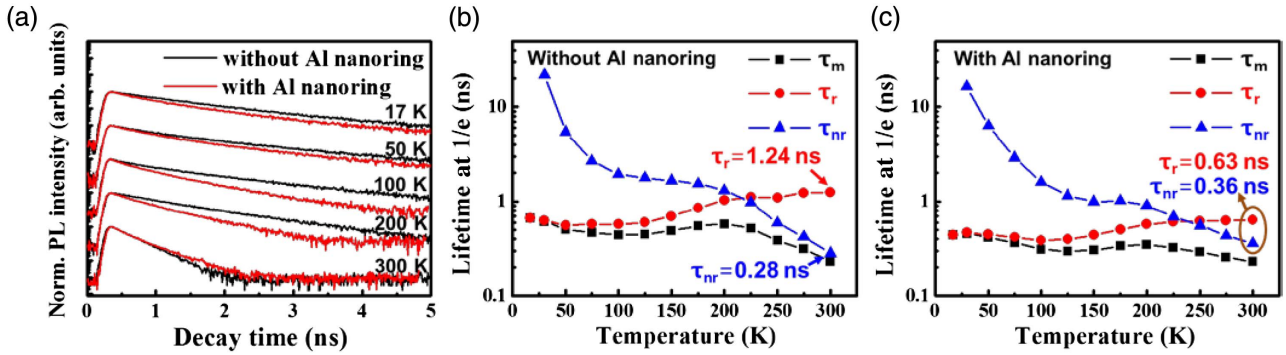

Fig. 5. (a) Temporal evolution of MQW emissions obtained at different temperatures for AlGaN/GaN MQW samples with and without Al nanoring structures. For both samples, temporal curves are normalized and vertically shifted for comparison. Measured PL lifetime τ_m and radiative and nonradiative lifetimes (τ_r and τ_{nr}) (b) without Al nanorings and (c) with Al nanorings inferred from the temperature-dependent time-resolved PL result and integrated PL intensity.

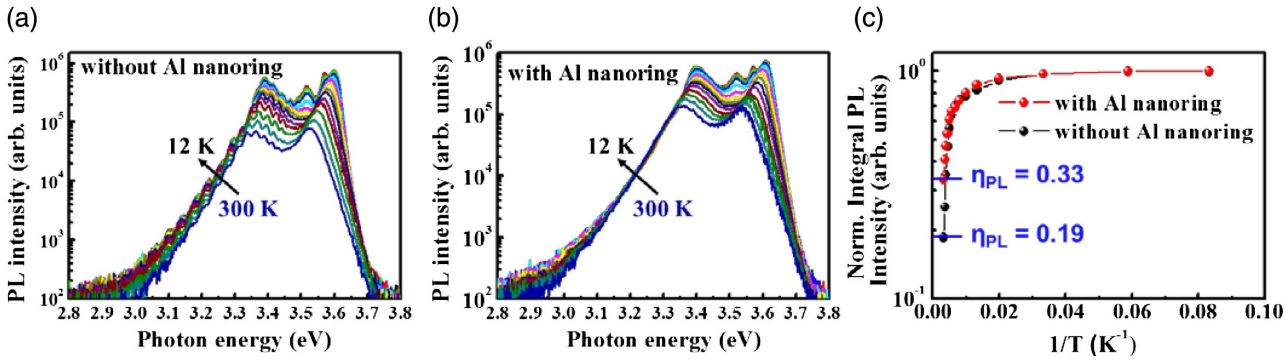

Fig. 6. TDPL measurements. PL spectra of AlGaN/GaN MQW structures (a) without Al nanorings (b) with Al nanorings at temperatures from 12 to 300 K. (c) Arrhenius plot of the normalized integrated PL intensities for AlGaN/GaN MQWs with and without Al nanorings.

surface defects [30]. During the dry-etching process, the crystalline quality of the sample can be degraded by producing some defects at the surface. These defects can act as nonradiative recombination or trapping centers. However, these surface defects can be reduced by passivation effects through the Al nanorings. In other words, by adding the Al nanorings, the total number of photons contributing to the radiative recombination process increases by surface passivation, eventually leading to the increase of the radiative recombination rate ($\tau_r \downarrow$) and the decrease of the nonradiative recombination rate ($\tau_{nr} \uparrow$). Therefore, PL decay rates of the sample with Al nanorings became lower than those of the sample without Al nanorings, although the radiative recombination rate increased. This is why the τ_m of the sample with Al nanorings becomes almost identical with that of the sample without Al nanorings, as shown in Fig. 4(b). In conclusion, the spontaneous emission rate was enhanced for the sample with Al nanorings, and this enhancement can clearly be attributed to LSP-QW coupling.

Further, the radiative to nonradiative transition behavior occurs at a lower temperature of 215 K for the sample without Al nanorings and at a higher temperature of 235 K for that with Al nanorings. By comparing both results with temperature, we can deduce that the formation of Al nanorings in AlGaN/GaN MQWs leads to not only an increased radiative recombination rate of excitons due to the Purcell effect of LSP-QW coupling but also a variation in the nonradiative recombination process caused by metallic quenching and/or nanoring patterns on the surface.

The PL intensities of the AlGaN/GaN MQW samples with and without Al nanorings were measured from 12 to 300 K to characterize the optical properties, as shown in Figs. 6(a) and 6(b). Then, we defined the PL efficiency (η_{PL}) as the relative ratio of PL intensities between a given temperature T and 12 K, as

$$\eta_{PL}(T) = I(T)/I_{12\,K}. \quad (4)$$

As a result, the calculated PL efficiency at room temperature at 3.36 eV (both with and without Al nanorings) is 0.33 and 0.19, respectively, as shown in Fig. 6. In terms of PL efficiency, the approximately 1.73-fold enhancement was obtained at room temperature, which implies that the AlGaN/GaN MQW structure with Al nanorings has a higher IQE when compared with that without Al nanorings. This enhancement ratio is found to be higher than what has been reported in the literature (i.e., 1.35-fold for colloidal Ag nanoparticles [15]; 1.63-fold for Al nanospheres [18] when these structures were applied to UV-LEDs). Therefore, we believe that the use of nanoring structures are quite useful to enhance the quantum efficiency of UV LEDs.

4. CONCLUSIONS

We fabricated Al nanoring arrays on top of an AlGaN/GaN MQW structure to enhance the IQE of LEDs that have a wavelength of 365 nm using LSP-QWs. Through 3D FDTD simulations, we confirmed that the Al nanoring array of the HCP structure is characterized by the dramatic enhancement in the electric field on the outer surface caused by interactions between the rings. Compared with the bare MQW structure, the emission enhancement ratio of 227% in peak PL intensity was obtained at a source power of 0.03 mW. As a result of TDPL and time-resolved PL measurements, the calculated PL efficiencies at room temperature for the structure with and without Al nanorings were 33% and 19%, respectively. In addition, the calculated radiative lifetimes were 0.63 and 1.24 ns for the structure with and without Al nanorings, respectively, at room temperature. Therefore, the enhanced spontaneous emission rate due to LSP-QW coupling together with nanoring pattern formation on the surface play key roles in the overall optical properties of MQWs with Al nanoring structures.

Funding. National Research Foundation of Korea (NRF) (2016R1A3B 1908249).

REFERENCES

1. P. Yeh, N. Yeh, C.-H. Lee, and T.-J. Ding, "Applications of LEDs in optical sensors and chemical sensing device for detection of biochemical, heavy metals, and environmental nutrients," Renew. Sustain. Energy Rev. **75**, 461–468 (2017).
2. H.-Y. Lin, C.-W. Sher, D.-H. Hsieh, X.-Y. Chen, H.-M. P. Chen, T.-M. Chen, K.-M. Lau, C.-H. Chen, C.-C. Lin, and H.-C. Kuo, "Optical cross-talk reduction in a quantum-dot-based full-color micro-light-emitting-diodes display by a lithographic-fabricated photoresist mold," Photon. Res. **5**, 411–416 (2017).

3. K. Song, M. Mohseni, and F. Taghipour, "Application of ultraviolet light-emitting diodes (UV-LEDs) for water disinfection: a review," Water Res. **94**, 341–349 (2016).
4. Y. Muramoto, M. Kimura, and S. Nouda, "Development and future of ultraviolet light-emitting diodes: UV-LED will replace the UV lamp," Semicond. Sci. Technol. **29**, 084004 (2014).
5. M. Krames and N. Grandjean, "Light-emitting diodes technology and applications: introduction," Photon. Res. **5**, LED1–LED2 (2017).
6. J. S. Speck and S. J. Rosner, "The role of threading dislocations in the physical properties of GaN and its alloys," Physica B **273–274**, 24–32 (1999).
7. T. Sugahara, H. Sato, M. Hao, Y. Naoi, S. Kurai, S. Tottori, K. Yamashita, K. Nishino, L. T. Romano, and S. Sakai, "Direct evidence that dislocations are non-radiative recombination centers in GaN," Jpn. J. Appl. Phys. **37**, L398–L400 (1998).
8. N. Grandjean, B. Damilano, S. Damasso, M. Leroux, M. Laugt, and J. Massies, "Built-in electric-field effects in wurtzite AlGaN/GaN quantum wells," J. Appl. Phys. **86**, 3714–3720 (1999).
9. A. Bryan, I. Bryan, J. Xie, S. Mita, Z. Sitar, and R. Collazo, "High internal quantum efficiency in AlGaN multiple quantum wells grown on bulk AlN substrates," Appl. Phys. Lett. **106**, 142107 (2015).
10. F. Wu, H. Sun, I. A. AJia, I. S. Roqan, D. Zhang, J. Dai, C. Chen, Z. C. Feng, and X. Li, "Significant internal quantum efficiency enhancement of GaN/AlGaN multiple quantum wells emitting at ~350 nm via step quantum well structure design," J. Phys. D **50**, 245101 (2017).
11. E. C. Young, B. P. Yonkee, F. Wu, B. K. Saifaddin, D. A. Cohen, S. P. DenBaars, S. Nakamura, and J. S. Speck, "Ultraviolet light emitting diodes by ammonia molecular beam epitaxy on metamorphic AlGaN/GaN buffer layers," J. Cryst. Growth **425**, 389–392 (2015).
12. T. Takano, T. Mino, J. Sakai, N. Noguchi, K. Tsubaki, and H. Hirayama, "Deep-ultraviolet light-emitting diodes with external quantum efficiency higher than 20% at 275 nm achieved by improving light-extraction efficiency," Appl. Phys. Express **10**, 031002 (2017).
13. K. Okamoto, I. Niki, A. Shvartser, Y. Narukawa, T. Mukai, and A. Scherer, "Surface-plasmon-enhanced light emitters based on InGaN quantum wells," Nat. Mater. **3**, 601–605 (2004).
14. M.-K. Kwon, J.-Y. Kim, B.-H. Kim, I.-K. Park, C.-Y. Cho, C. C. Byeon, and S.-J. Park, "Surface-plasmon-enhanced light-emitting diodes," Adv. Mater. **20**, 1253–1257 (2008).
15. S.-H. Hong, J.-J. Kim, J.-W. Kang, Y.-S. Jung, D.-Y. Kim, S.-Y. Yim, and S.-J. Park, "Enhanced optical output of InGaN/GaN near-ultraviolet light-emitting diodes by localized surface plasmon of colloidal silver nanoparticles," Nanotechnology **26**, 385204 (2015).
16. K. Huang, N. Gao, C. Wang, X. Chen, J. Li, S. Li, X. Yang, and J. Kang, "Top- and bottom-emission-enhanced electroluminescence of deep-UV light-emitting diodes induced by localized surface plasmons," Sci. Rep. **4**, 4380 (2014).
17. J. Yin, Y. Li, S. Chen, J. Li, J. Kang, W. Li, P. Jin, Y. Chen, Z. Wu, J. Dai, Y. Fang, and C. Chen, "Surface plasmon enhanced hot exciton emission in deep UV-emitting AlGaN multiple quantum wells," Adv. Opt. Mater. **2**, 451–458 (2014).
18. C. Zhang, N. Tang, L. Shang, L. Fu, W. Wang, F. Xu, X. Wang, W. Ge, and B. Shen, "Local surface plasmon enhanced polarization and internal quantum efficiency of deep ultraviolet emissions from AlGaN-based quantum wells," Sci. Rep. **7**, 2358 (2017).
19. S.-I. Inoue, T. Naoki, T. Kinoshita, T. Obata, and H. Yanagi, "Light extraction enhancement of 265 nm deep-ultraviolet light-emitting diodes with over 90 mW output power via an AlN hybrid nanostructure," Appl. Phys. Lett. **106**, 131104 (2015).
20. S.-I. Inoue, N. Tamari, and M. Taniguchi, "150 mW deep-ultraviolet light-emitting diodes with large-area AlN nanophotonics light-extraction structure emitting at 265 nm," Appl. Phys. Lett. **110**, 141106 (2017).
21. Q.-A. Ding, K. Li, F. Kong, J. Zhao, and Q. Yue, "Improving the vertical light extraction efficiency of GaN-based thin-film flip-chip LED with double embedded photonics crystals," IEEE J. Quantum Electron. **51**, 3300109 (2015).
22. E. Prodan, C. Radloff, N. J. Halas, and P. Nordlander, "A hybridization model for the plasmon response of complex nanostructures," Science **302**, 419–422 (2003).
23. P. Nordlander, "The ring: a leitmotif in plasmonics," ACS Nano **3**, 488–492 (2009).
24. J. M. Sanz, D. Ortiz, R. Alcaraz de la Osa, J. M. Saiz, F. Gonzalez, A. S. Brown, M. Losurdo, H. O. Everitt, and F. Moreno, "UV plasmonic behavior of various metal nanoparticles in the near and far-field regimes: geometry and substrate effects," J. Phys. Chem. C **117**, 19606–19615 (2013).
25. C. L. Haynes and R. P. Van Duyne, "Nanosphere lithography: a versatile nanofabrication tool for studies of size-dependent nanoparticle optics," J. Phys. Chem. B **105**, 5599–5611 (2001).
26. Z. Bai, G. Tao, Y. Li, J. He, K. Wang, G. Wang, X. Jiang, J. Wang, W. Blau, and L. Zhang, "Fabrication and near-infrared optical responses of 2D periodical Au/ITO nanocomposite arrays," Photon. Res. **5**, 280–286 (2017).
27. E. Prodan and P. Nordlander, "Electronic structure and polarizability of metallic nanoshells," Chem. Phys. Lett. **352**, 140–146 (2002).
28. S. F. Chichibu, M. Sugiyama, T. Onuma, T. Kitamura, H. Nakanishi, T. Kuroda, A. Tackeuchi, T. Sota, Y. Ishida, and H. Okumura, "Localized exciton dynamics in strained cubic $In_{0.1}Ga_{0.9}N$/GaN multiple quantum wells," Appl. Phys. Lett. **79**, 4319–4321 (2001).
29. Y.-H. Cho, G. H. Gainer, A. J. Fischer, J. J. Song, S. Keller, U. K. Mishra, and S. P. DenBaars, ""S-shaped" temperature-dependent emission shift and carrier dynamics in InGaN/GaN multiple quantum wells," Appl. Phys. Lett. **73**, 1370–1372 (1998).
30. W. F. Yang, Y. N. Xie, R. Y. Liao, J. Sun, Z. Y. Wu, L. M. Wong, S. J. Wang, C. F. Wang, A. Y. S. Lee, and H. Gong, "Enhancement of bandgap emission of Pt-capped MgZnO films: important role of light extraction versus exciton-plasmon coupling," Opt. Express **20**, 14556–14563 (2012).